Engineering Conferences International
ECI Digital Archives

The 14th International Conference on Fluidization
– From Fundamentals to Products

Refereed Proceedings

DEM Simulations of Fluidized Beds Including Heat Transfer

A.V. Patil
Technical University Eindhoven, Netherlands

E.A.J.F. Peters
Technical University Eindhoven, Netherlands

M. van der Hoef
Technical University Eindhoven, Netherlands

J.A.M. Kuipers
Technical University Eindhoven, Netherlands

DEM simulations of fluidized beds including heat transfer

Patil, A.V.   Peters, E.A.J.F.   Hoef, M. van der
Kuipers, J.A.M.
Dept. of Chemical Eng. and Chemistry, Technical University Eindhoven,
P.O. Box 513, 5600 MB Eindhoven, The Netherlands

March 12, 2013

Abstract

Discrete element method (DEM) simulations of a pseudo 2-D fluidized bed at non-isothermal conditions are presented. Hot gas is injected in a colder bed that is close to minimum fluidization conditions. Following a verification of the implementation bubbles formed in monodisperse beds of different particle sizes ($1\,mm$, $2\,mm$ and $3\,mm$) and with a range of injection temperatures (300 to $900\,K$) are analyzed.

1   Introduction

Fluidized beds with gas-solid flows are widely used in a variety of process industries. Until recently simulation of fluidized beds mainly focused on the hydrodynamics. Now with proper understanding of hydrodynamics the frontier has moved towards heat transfer. This work focuses on modeling of heat transfer in fluidized beds using the discrete element method (DEM). Experimental research on heat transport inside a fluidized beds has many obstacles, but a simulation approach like presented here (DEM) has the capability to predict hydrodynamic and thermal properties in great detail and thus provide the needed insight.

The hydrodynamics of gas-solid flow in DEM is modeled by treating the gas phase as a continuum (Eulerian) and particulate phase as discrete (Lagrangian). Both the continuum and particulate phase experience each other through momentum coupling. To the existing hydrodynamic model, heat transfer is added where convection (forced and free) and conduction in the gas-phase are taken into account.

The developed heat transport model is verified by comparison of a simple case with analytical solutions prior to study of fluidized beds. Using the developed model bubble injection into a 2-D bed was performed and the rising bubble analyzed. The study includes variations with changing particle sizes and gas injection temperatures. The mass flux of bubble is fixed to isolate the temperature dependence of the evolution of the formed bubble.

2   Governing Equations

2.1   Gas phase modeling

In the discrete element model the fluid phase is considered to be continuous. The governing equations are the continuity equation and Navier-Stokes equation described in eq. (1). For the cases where the fluid is a gas it is assumed to be compressible and obeying the ideal

gas law. We will use the convention that fluid variables have no subscript and particle properties are indicated by a subscript p,

$$\frac{\partial}{\partial t}(\varepsilon\,\rho) + \nabla\cdot(\varepsilon\,\rho\,\bar{u}) = 0, \text{ and } \varepsilon\,\rho\,\frac{\mathrm{D}}{\mathrm{D}t}\bar{u} = -\varepsilon\,\nabla P - \nabla\cdot(\varepsilon\,\bar{\bar{\tau}}) - \bar{S}_p + \varepsilon\,\rho\,\bar{g} \qquad (1)$$

where the particle-phase porosity, ε_p, the source term for momentum from the particulate phase, $\bar{S}_p$, are given by

$$\varepsilon_p = 1 - \varepsilon = \sum_{a\in\text{cells}} V_a\,\delta(\bar{r} - \bar{r}_a), \text{ and } \bar{S}_p = \sum_{a\in\text{cells}} \frac{\beta\,V_a}{\varepsilon_p}\,(\bar{u} - \bar{v}_a)\,\delta(\bar{r} - \bar{r}_a) \qquad (2)$$

In the numerical implementation the Dirac-delta functions will be smoothed as to distribute particle properties over nearby grid-points. The energy transport equation for the fluid is given by,

$$\varepsilon\,\rho\,\frac{\mathrm{D}}{\mathrm{D}t}H = \nabla\cdot(\varepsilon\,k^{\text{eff}}\nabla T) + Q_p, \text{ with } k^{\text{eff}} = \frac{1 - \sqrt{\varepsilon_p}}{\varepsilon}k, \qquad (3)$$

The source term from inter-phase heat transport, Q_p, equals

$$Q_p = \sum_{a\in\text{cells}} Q_{p,a}\,\delta(\bar{r} - \bar{r}_a) = \sum_{a\in\text{cells}} h_{fp}A_a(T_a - T)\,\delta(\bar{r} - \bar{r}_a), \qquad (4)$$

where h_{fp} is particulate interfacial heat transfer coefficient which is defined by an empirical correlation given by Gunn [1], with, $\mathrm{Nu}_p = h_{fp}d_p/k$, $\mathrm{Re}_p = d_p\varepsilon\,\rho\,|\bar{u} - \bar{v}|/\mu$ and $\mathrm{Pr} = \mu\,C_p/k$, by

$$\mathrm{Nu}_p = (7 - 10\,\varepsilon + 5\,\varepsilon^2)[1 + 0.7\,\mathrm{Re}_p^{0.2}\,\mathrm{Pr}^{0.33}]$$
$$+ (1.33 - 2.40\,\varepsilon + 1.20\,\varepsilon^2)\,\mathrm{Re}^{0.7}\,\mathrm{Pr}^{0.33}. \qquad (5)$$

2.2 Discrete particle phase

The solid phase is considered to be discrete and non-penetrating. The modeling of the particle phase flow is based on tracking the motion of spherical particles due to various forces acting on them. The motion of a single spherical particle a with mass m_a and moment of inertia I_a can be described by Newtonian equations:

$$m_a\frac{\mathrm{d}^2\bar{r}_a}{\mathrm{d}t^2} = -V_a\,\nabla p + \frac{\beta V_a}{\varepsilon_p}\,(\bar{u} - \bar{v}_a) + m_a g + \bar{F}_{\text{contact},a}, \text{ and } I_a\frac{\mathrm{d}^2\Theta_a}{\mathrm{d}t^2} = \hat{T}_a, \qquad (6)$$

where $\bar{r}_a$ is the particle position and Θ_a the angular displacement. The forces are due to the pressure gradient, drag, gravity and contact forces due to collisions and $\hat{T}_a$ is the torque. The used particle-particle collisions is based on the soft sphere model first proposed by Cundall and Strack [2]. The heat transfer from the particles to the fluid is modeled for DEM is given by eq. (4), and the change of particle temperature $Q_{p,a} = -V_a\,\rho_p\,C_{p,p}\,\mathrm{d}T_a/\mathrm{d}t$.

3 Implementation test and verification

In this section we present a test of the heat transfer coupling implementation. Tests on the hydrodynamic part of the code are not presented here, but can be found in literature [3].

channel geom.	0.1 m × 0.1 m × 1.0 m				
particle arrangement	25 × 25 × 125				
v_{inlet}	0.1	m/s			
			d_p	3.95	mm
ρ	1000	kg/m^3	ρ_p	8400	kg/m^3
μ	0.001	Pa · s			
C_p	4187	J/kg K	$C_{p,p}$	385	J/kg K
k	0.5	W/m K			

Table 1: Properties and settings for the test problem of heating of a fixed bed.

For the heat transfer test case we choose water as the fluid and copper as the material of the solid particles. The geometry, particle size, packing and hydrodynamic fluid properties are taken identical to those used in the Ergun equation test in Ref. [3]. The hydrodynamic and thermal properties used are tabulated in Table 1.
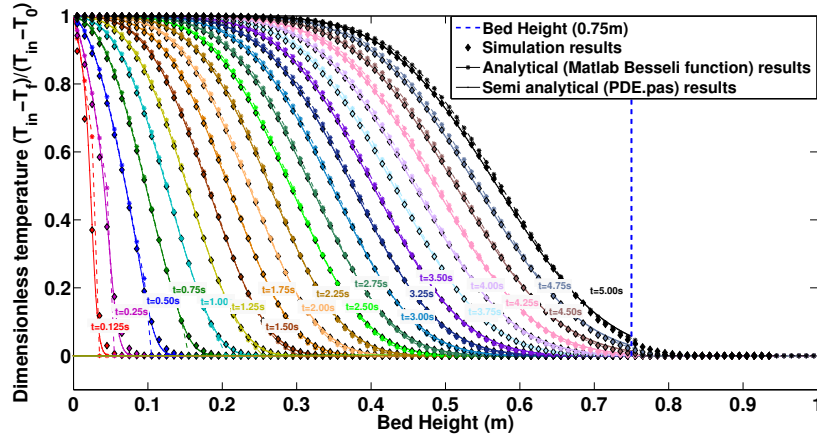

Figure 1: Temperature profile for the fluid in a packed bed that is heated-up by inflow of a hot fluid.

The test-problem that is considered is the heating of a packed bed initially filled with cold liquid by means of a hot liquid. Thus the temperature of the liquid in the bed rises causing the fixed particles also to heat up. The simulation results are compared to a one dimensional heat-transport problem with thermal conduction and axial dispersion terms neglected as they are bound to be small at high enough Peclet number. The model equations used are

$$\frac{\partial T}{\partial t} + u_z \frac{\partial T}{\partial z} = -\frac{h\,a}{\varepsilon\,\rho\,C_p}\,(T - T_p), \text{ and } \frac{\partial T_p}{\partial t} = \frac{h\,a}{\varepsilon_p \rho_p C_{p,p}}\,(T - T_p), \tag{7}$$

where a is the specific interfacial area given by $a = 6\varepsilon_p/d_p$. The analytical solution for this heat transfer problem can be found in references [4, 5, 6, 7]. Fig. 1 shows the DEM simulation results for the saturation for the fixed bed liquid phase. In the plot the results are compared with the analytic solution and with the solution of a 1-D discretized heat-transfer model (that includes conduction in the liquid phase and axial dispersion). The close agreement confirms that the implementation of heat-transfer in the DEM code is correct.
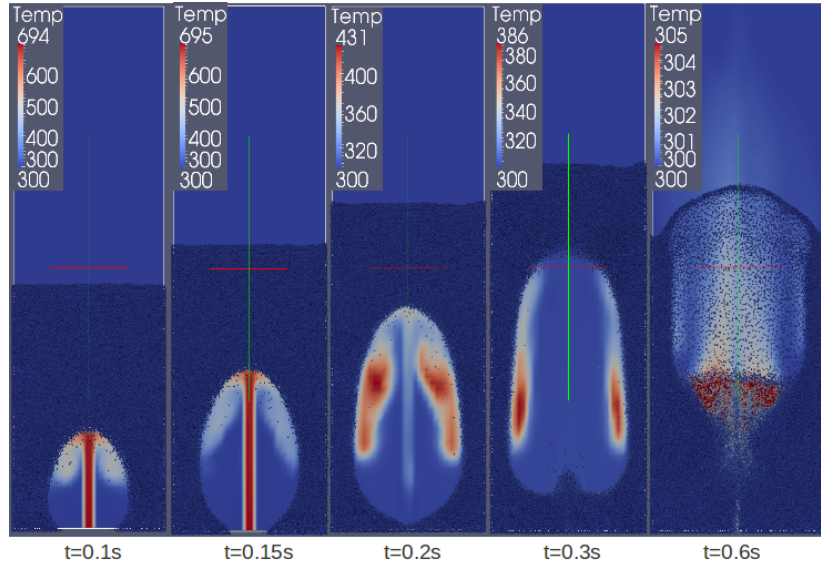
3

Figure 2: Gas bubble injection with 700 K gas injection in 300 K bed with varying scale. The injection is stopped at $t = 0.18$ s. The particle size is 2 mm.

4 Bubble formation by hot gas injection

Pseudo 2-D simulations of a bubble in a fluidized bed will subsequently be reported. Hot gas is injected into an incipiently fluidized bed. Table 2 contains the properties of the particles and other settings that were used in the simulation. Three particle sizes are considered. Some of the simulation parameters differ depending on the particle size.

material	glass
particle diameter	$1 - 3$ mm
particle density	2526 kg/m^3
norm. restit. coeff.	0.97
tang. restit. coeff.	0.33
$C_{p,p}$	840 J/kgK

d_p (mm)	u_{bg} (m/s)	bed depth (cm)	# particles
1	0.65	1.0	550000
2	1.1	1.5	100000
3	1.45	1.8	45000

Table 2: Particle properties and parameters that depend on particle size for fluidized bed simulations.

For the incipient fluidization the background fluidization gas temperature was kept at 300 K throughout all the simulations. The pseudo 2D-bed has a width of 21 cm and a depth that is different for different particle sizes (see Table 2). Through a central injection nozzle, with width 1.4 cm (and depth equal to the bed depth) air is injected with a mass flow 17.55 kg/m^{2}s at different temperatures and ambient pressure. The duration of the gas injection is 0.18 s facilitating the formation of single bubble. The temperatures considered are 300 to 900 K. The mass density and inlet velocities directly follow from the ideal gas-law.

Figure 2 shows snapshots of a simulation at 700 K. This figure shows how the temperature profile develops inside a rising gas bubble. Because the gas transfers its heat efficiently to the particles the temperature drops quickly to 300 K. As the temperature of gas in the
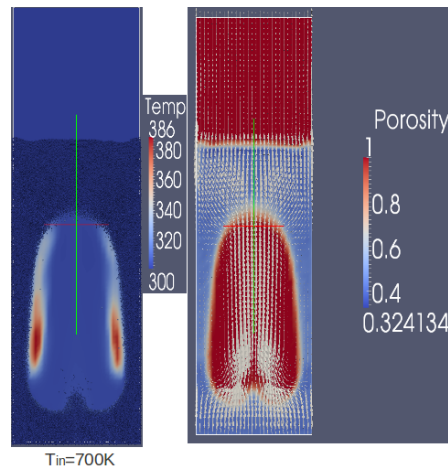
4

Figure 3: Gas bubble at time $t = 0.3$ s for 700 K injection with velocity field

bubble reduces quickly a new temperature scale is used for each snapshot.

The hottest part of the gas is near the boundary of the bubble. The hot gas tends to accumulate on the sides of the bubble as the background low temperature gas moves up through the center of the bubble. The temperature field along with the gas velocity field at $t = 0.3$ s that is shown in figure 3 gives a better understanding of this behavior. It shows how the background gas, that is used to keep the bed fluidized, flows through the bubble.

In figure 4 snapshots of bubbles at the same instant in time $(0.3$ s$)$ created with air injected at different temperatures are shown. The amount of gas injected in terms of mass is the same, so this corresponds to the same volume once cooled down to 300 K. The fact that the observed bubble is bigger for the higher temperatures can be explained by the fact that the injection velocity (volumetric flow rate) is higher. This means that the amount of momentum supplied by the injection is larger for higher temperatures.

The gas that is in contact with the emulsion phase is quickly cooled down by the particles. Since the glass particles used in these simulation have a high heat capacity, especially if one compares the heat-capacity per unit volume with that of the gas-phase, their temperature does not rise much. The maximum temperatures that some particles achieve due to direct contact with the hot injection gas in the hot gas bubble is approximately 320 to 370 K depending on the injection gas temperature. In the last snapshot of figure 2 for time $(0.6$ s$)$ it can be seen that after a while, when hot gas in the bubble has nearly escaped, the slightly warmer particles with maximum temperature of 305 K supply heat to the background cold gas flowing past them.

In figure 5 the time-evolution of the bubble size for several injection temperatures and particle sizes is shown. The size of the bubble is expressed in terms of an effective bubble diameter, i.e. the diameter of a cylinder with the same volume. The graphs initially show a linear growth. Note that the gas injection is stopped at $t = 0.18$ s, but the bubbles still grow somewhat after that time. Beyond, say $t = 0.25$ s, the bubble sizes are nearly constant. Note, however, that the data-points at later times are less trustworthy because of the difficulty of defining the bubble volume when particles are raining down from the roof of the bubble. The bubble size for isothermal injection at 300 K in the plot of figure 5 matches well with results previously published in the literature [8].

Bubbles are larger for higher injection temperatures and smaller particle sizes. For larger
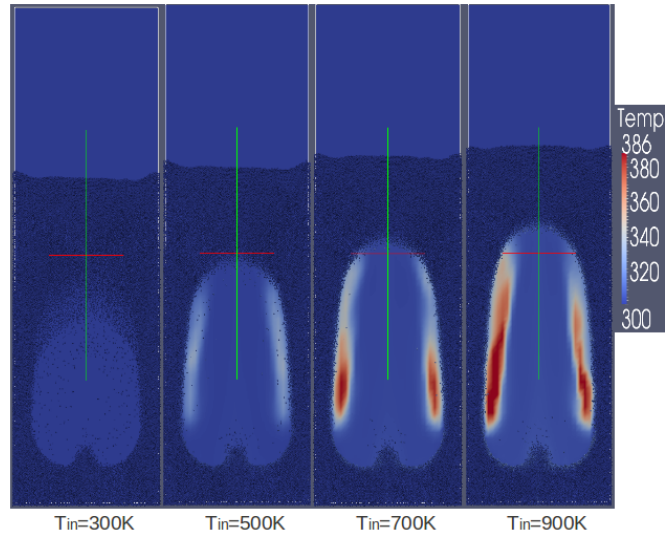
5

Figure 4: Gas bubble at time t=0.3s with varying injection temperature (with the same temperature scale for all snapshots).
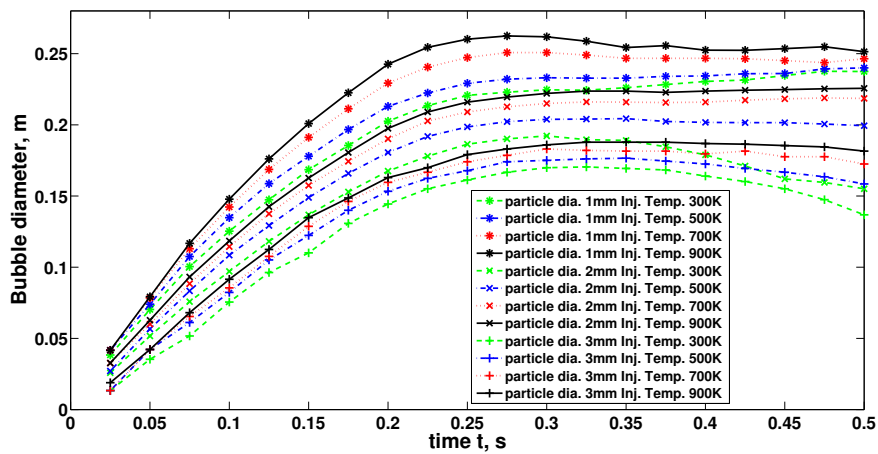

Figure 5: Effective bubble diameter varying with time for several injection temperature
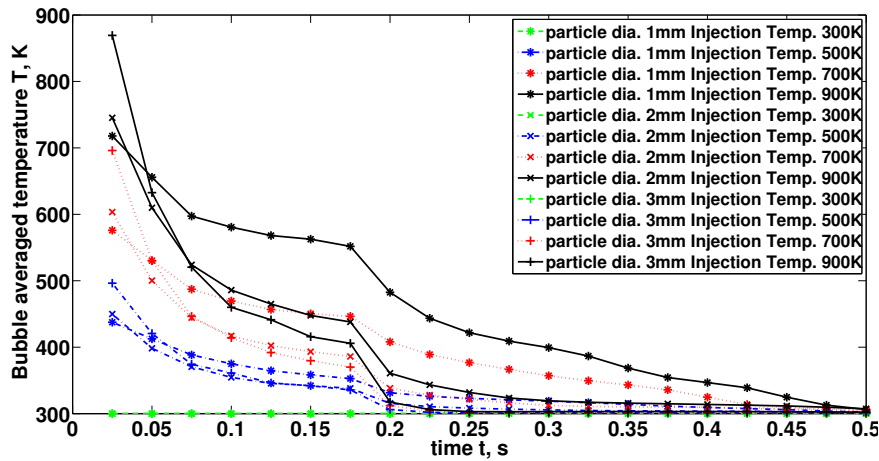
Figure 6: Bubble temperature variation with time for varying injection temperature

particles the resistance of the air flowing in and out of a bubble is less. Therefore the 'gas-leakage' out of the bubble is larger for systems with larger particles and bubble sizes will be smaller. The graphs in figure 5 show that for smaller particle diameters the leakage reduces with increasing injection temperature causing greater hot gas conservation in the bubble and thus resulting in a larger bubble size.

The mean averaged temperature of the bubble with respect to time is shown in figure 6. Let's focus on the 900 K case. It is seen that initially the temperature at 0.025 s in the 1 mm particle bed is lowest. The reason is that for these small particles the gas leakage out of the bubble is least. This means that hot gas that is cooled down by the particles remains (partially) in the bubble and decreases the temperature almost immediately. For the larger particles the gas is also cooled down but is easily convected away from the bubble into the bed. Therefore, initially, the bubble temperature is nearly equal to the injection temperature for the larger, 3 mm, particle system.

After this initial stage, while still injecting hot gas, there is much more leakage in and out of the bubble in case of the larger particles. In fact there is a flow that transports cold background gas into the bubble. This mixing in of cold gas causes the temperature inside the bubble to decrease quicker for the large particles.

When the injection is stopped the temperature initially drops very fast. This drop is largest for the large particle systems. The reason is that the hot gas (at the top) leaks out quickly. The snapshots, such as in figs. 2, 3 and 4, suggest that the remaining hot gas is in nearly stagnant zones near the sides of the bubble. Due to the stagnant character of the remaining warm zones the cooling down after the initial quick drop is much slower.

5 Conclusion

A proper incorporation of heat transfer in a DEM code has been achieved. This has been verified by a transient simulation of a fixed bed that is heated up by inflow of hot fluid. These simulations give a good match with the analytical solution and numerical solutions of an approximate 1-D model.

The model has been successfully used for a bubble-injection study where the temperature of the gas is varied. At a fixed mass flux it has been observed that the size of a bubble in a

7

fluidized bed is affected by both the injection gas temperature and particle size. This first study shows a complex interplay of conductive and convective heat transport that requires further investigation.

Acknowledgment

Notation

		a	specific interfacial area
		A_a	area of particle a
$\bar{\bar{\tau}}$	Newtonian stress tensor	C_p	fluid heat capacity per unit mass
$\bar{F}_a$	force on particle a	$C_{p,p}$	particle heat capacity per unit mass
$\bar{g}$	gravitational acceleration	d_p	particle diameter
$\bar{S}_p$	body force exerted by particles on fluid	H	fluid enthalpy per unit mass
		h_{fp}	heat transfer coefficient particles-fluid
$\bar{u}$	fluid velocity		
$\bar{v}_a$	velocity particle a	I_a	moment of inertia particle a
$\hat{T}_a$	torque on particle a	k^{eff}	effective thermal conductivity
Nu_p	particle Nusselt number	m_a	mass particle a
Pr	Prandtl number	P	pressure
Re_p	particle based Reynolds number	$Q_{p,a}$	heat flow from particle a to fluid
ρ	fluid mass density	Q_p	heat flow per unit volume from particles to fluid
ρ_p	particle mass density		
Θ_a	angular velocity particle a	T	temperature particle a
ε	fluid volume fraction	T	temperature
ε_p	particle volume fraction	V_a	volume particle a

References

[1] D.J. Gunn. Transfer of heat or mass to particles in fixed and fluidised beds. *Int. J. Heat and Mass Transfer*, 21:467–476, 1978.

[2] P.A. Cundall and O.D.L. Strack. A discrete numerical model for granular assemblies. *Geotechnique*, 29(1):47–65, 1979.

[3] M. Sint Annaland van., N.G. Deen, and J.A.M. Kuipers. Numerical simulation of gas-liquid-solid flows using a combined front tracking and discrete particle method. *Chemical Engineering Science*, 60(22):6188–6198, 2005.

[4] A. Anzelius. Über erwärmung vermittels durchströmender medien. *J. Applied Mathematics and Mechanics*, 6(4):291–294, 1926.

[5] H. Bateman. *Partial Differential Equations of Mathematical Physics*. Cambridge University Press, 1932.

[6] O.A. Hougen and K.M. Watson. *Chemical Process Principles: Kinetics and Catalysis*. Chemical Process Principles. Wiley, 1947.

[7] Bird R.B., Stewart W.E., and Lightfoot E.N. *Transport phenomena*. John Wiley and Sons, 2001.

[8] O.O. Olaofe, M.A. van der Hoef, and J.A.M. Kuipers. Bubble formation at a single orifice in a 2d gas fluidised beds. *Chem. Engg. Sci.*, 66:2764–2773, 2011.